DESIGN AND ANALYSIS OF A SOFT SPIRAL GRIPPER

BY

NAVEEN KUMAR UPPALAPATI

THESIS

Submitted in partial fulfillment of the requirements
for the degree of Master of Science in Systems and Entrepreneurial Engineering
in the Graduate College of the
University of Illinois at Urbana-Champaign, 2016

Urbana, Illinois

Adviser:

Assistant Professor Girish Krishnan

Abstract

Continuum robots have been gaining popularity in recent years for their umpteen advantages. Soft robots are a class of continuum robots which are made of squishy materials which have the added benefit of being innocuous to humans. Soft robotic grippers are one of the major application of soft robots as they have the ability to conform and adapt their structure to the object to be grasped.

This work presents a bio-inspired technique to increase contact area while grasping and handling long slender objects by helically twisting around them. An embodiment of such a spiral gripper utilizes unique configurations of pneumatically actuated Fiber Reinforced Elastomeric Enclosures which has a range of motions like extension, rotation, contraction. This work presents a detailed analysis technique using Cosserat beam theory to estimate the normal contact force exerted by the spiral gripper on cylindrical objects.

To my teacher, who gave me the right vision

Acknowledgements

First, I would like to acknowledge my teacher for educating me with the proper use of education. His vision and example is what has inspired me to choose higher studies after receiving my bachelor's degree.

I was fortuitous to have Dr. Girish Krishnan as my advisor. Right from the beginning he has been very patient and encouraging. He spent a lot of time in transforming me from an undergraduate student to a researcher. Discussions with him have made my thoughts coherent and clear. Without his expert guidance and support I wouldn't have done this work.

My colleagues in Monolithic Systems Lab (MSL), starting from Gaurav, Zhang, Sree Kalyan and Sree Shankar have always been very helpful and friendly. They patiently heard my ideas and gave their insightful comments. I have learnt the art of designing and performing new experiments from them. We had a great team of undergraduates with Hugo, Jacob and Luke who have been ready with prototypes when needed.

I am also very grateful to my friends here at Urbana, they have created a more than home like environment and assisted me to focus on higher purpose. Their heartwarming support was the reason for my smooth transition after I came here.

I am very grateful to my parents and sister for their love and blessings. They have supported my decisions even during some difficult phases of their life. Its their upbringing which has assisted me immensely. I am very grateful to the Supreme Lord for his protection throughout.

Table of Contents

List of Figures

1 INTRODUCTION

Unlike rigid robots, continuum flexible robots are increasingly becoming popular for their advantage of operation in unstructured terrains [5] [6]. Recently, there has been a rise in use of these continuum robots for various medical applications [7] and military applications [8]. Soft continuuum flexible robots are a class of these continuum robots which are composed of soft actuators. This 'soft' nature has gained them immense interest in recent years, as they can interact safely with humans and environment [9] [10]

These soft robots have been successfully demonstrated to perform various locomotion [11] [12] and manipulation tasks, which largely includes gripping and grasping [13] [14]. As the name suggests soft robots inherently don't possess the large stiffness needed to hold heavy objects, unless they are stiffened by granular materials [15] [16].

Soft grippers generally adapt and conform to the shape of the objects that they manipulate, thus creating a stable grasp. Larger the contact surface, larger is the stability of grasp. In conventional rigid-link robotics, researchers have used the concept of whole arm grasping to good effect [17]. Here, the entire body of the robot is involved in grasping. In nature, octopuses, grape-wine tendrils and squids spirally twist their tentacles around their long and slender prey to maximize gripping force [18] [2]. Recently, there have been a number of soft robots shown in Fig. 1.1 that claim whole arm grasping of long and slender objects [4] [3] [1] [19]. In these works the focus has been on design of a spiral soft robot to accomplish different tasks. In this work we present the design, analysis and testing of a soft spiral gripper that twists around long and slender objects to maxi-

mize the grip. The gripper is pneumatically actuated and is made up of Fiber Reinforced Elastomeric Enclosures (FREEs) [20]. FREEs are hollow elastomeric tubes whose spatial motion pattern is a function of the fluid pressure and the reinforced fiber orientations. Earlier versions of spiral helical actuators were presented in [19] with simplistic analytical equations to explain its behavior without the inclusion of realistic conditions such as contact forces, gravity and material properties. In this work, we present a geometrically exact method [21] to analyze spiral FREE-based actuators, and use this to estimate the gripping force on a cylinder surface. This analysis framework is deemed to be useful in exploring the design space of spiral actuators, and specifically to synthesize a gripper for maximum gripping force, stability and adaptability. There has also been work on probabilistic force sensing on continuum robots by Rucker et al. [22] in which only tip force is estimated.

1.1 Scope

The main objective of this work is to extend the Cosserat rod framework to FREE based spiral actuator and to estimate the force exerted by the spiral actuator on the cylindrical object. The design is limited to use of FREE as the basis actuator but the analysis presented in this work can be used to any spiral soft actuator which uses its entire or portion of length for grasping objects. The main contributions of this work can be summarized as:

- A new soft spiral actuator based on FREEs which can be used for grasping long and cylindrical objects.
- Use of geometric exact model framework for FREE based spiral actuator.

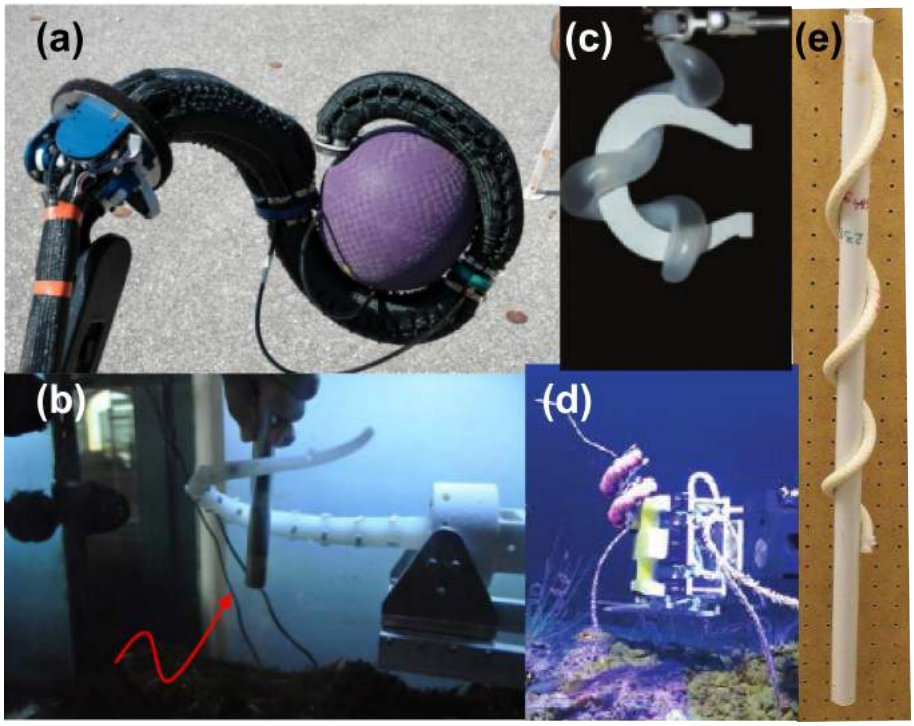

Figure 1.1: (a) Whole arm grasping used in various soft actuators (a) Octarm [1] (b) Octopus [2] (c) 3D robotic tentacle [3] (d) Boa-type gripper [4] and (e) FREE based spiral actuator (this work)

- Method to estimate the forces exerted by the spiral actuator on the cylindrical object.

1.2 Outline

This thesis is organized as follows.

In Chapter 2, first a brief review of FREEs which are the building blocks for soft robots is presented. Then using the design space of FREEs design of a spiral actuator is detailed and finally a brief procedure of the fabrication used in this work is presented.

In Chapter 3, the modeling of FREE based spiral actuator is presented. The kinematic equations and mechanics which facilitate the functionality of this actuator is explained along with the numerical methods used to obtain a solution .

In Chapter 4, an algorithm for predicting the normal forces exerted on the spiral ac-

tuator by a cylindrical object is presented. The different cases possible are presented and modification in algorithm to comply with these cases is also detailed

In Chapter 5 the conclusions, future work along with an application is presented .

2 FREE BASED SPIRAL ACTUATOR DESIGN

In this chapter, firstly a novel pneumatic soft actuator termed as Fiber Reinforced Elastomeric Enclosures(FREEs) is presented and then details about the design of spiral soft actuator and its fabrication are discussed.

2.1 FREEs: Building blocks for soft robots

Fiber Reinforced Elastomeric Enclosures (FREEs) are quintessential building blocks for soft robotics, as they encapsulate fundamental constituents of recurrent designs in literature and nature [20,23]. These designs include stretchable skin enclosures reinforced with inextensible fibers that contain pressurized fluids. The interaction of these constituents lead to complex deformed shapes that can be leveraged to perform mechanical tasks in soft robots.

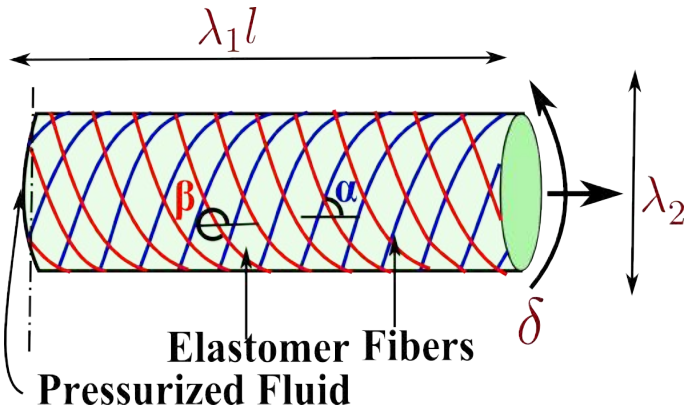

Figure 2.1: Structure of a regular FREE

The most simplified representation of a FREE is a hollow cylinder made of stretchable elastomer material and reinforced with two families of fibers denoted by angles α and

β respectively as shown in Fig. 2.1. These are inspired in construction and operating principle by well-known pneumatic artificial muscles or McKibben actuators [24, 25]. While McKibben actuators either contract or extend upon pressurization, FREEs can also undergo axial rotation as shown in Fig.2.3(b). It is the repository of these deformation modes that can be leveraged to design novel soft robots.

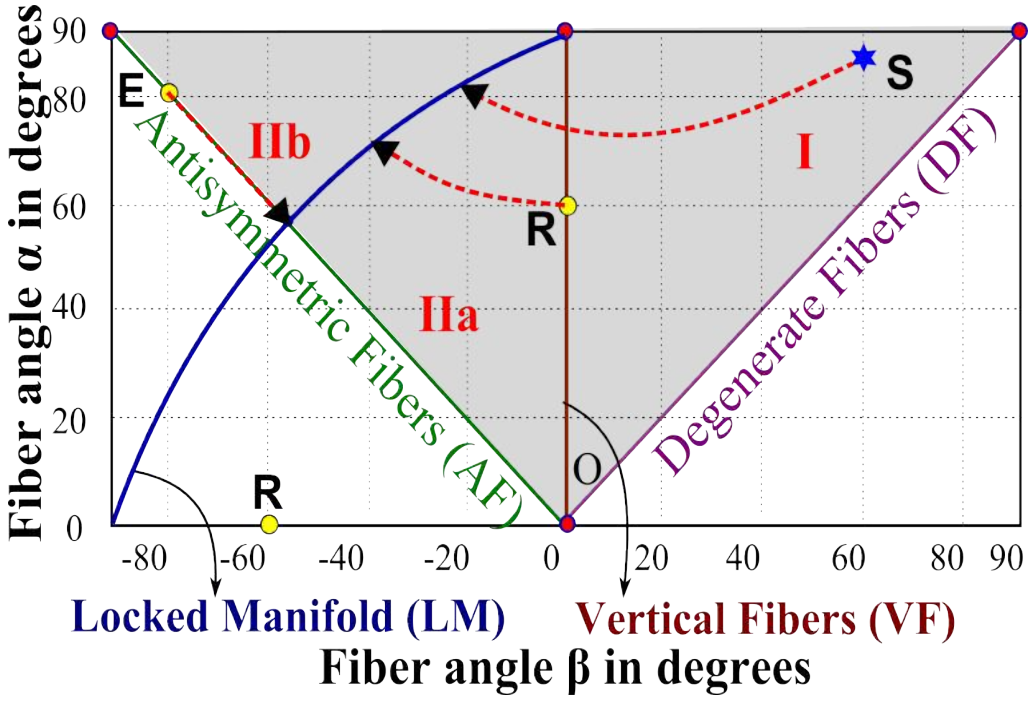

Figure 2.2: Fiber Reinforced Elastomeric Enclosures (FREEs) Design space spanned by the two fiber angles

Simple reduced order models show that two families of helically wound fibers yield a kinematically well-constrained system (Fig.2.1) [20,23]. Due to this kinematic constraint of the system, the actuator's performance is less influenced by material imperfections. These two families of fibers span a design space denoted by angles α and β respectively as shown in Fig.2.2. It must be recognized that the popular configuration of contracting McKibben actuators [24, 25] spans just a line (α = - β line shown in green in Fig.2.2. as Antisymmetric fibers AF).

Governing Equations: The governing equations for FREEs are greatly simplified by as-

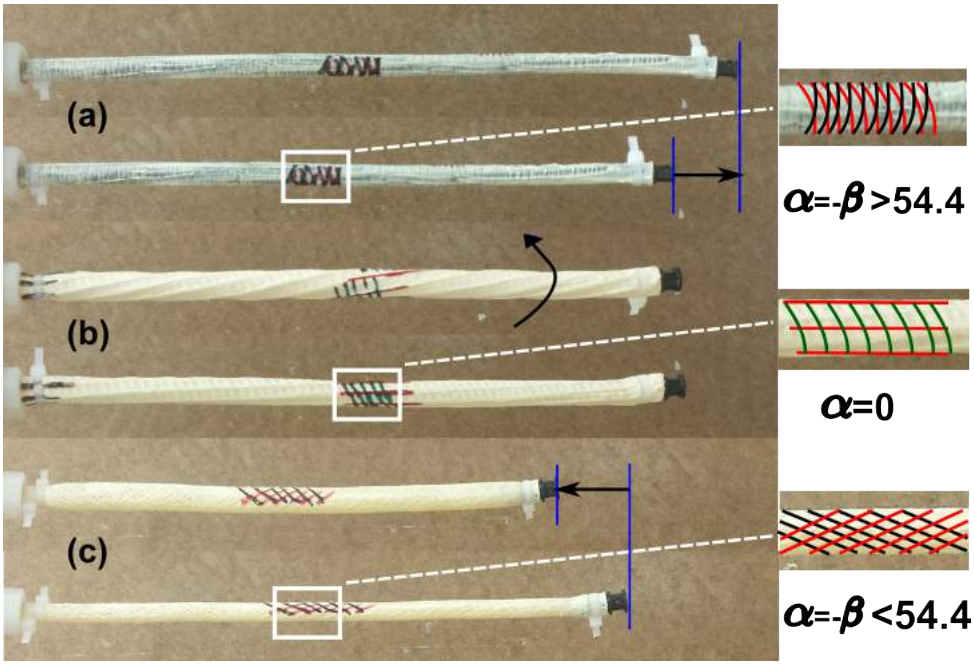

Figure 2.3: (a)FREE undergoing extension, (b) Rotation and (c) Contraction with fiber angles in inset

suming cylindrical geometry for both the deformed and undeformed configurations. The deformation parameters are represented as stretch ratios λ_1 and λ_2 (see Fig. 2.1), which are ratios of the deformed to undeformed length and diameters respectively. Furthermore, it is assumed that the fibers are inextensible and this leads to two equations as shown in Eq 2.1 that maintains this constraint in any configuration. In this equation, α and β are the fiber angles and δ is the axial rotation of the FREE. θ and ϕ are the number of turns due to each family of fiber (see [20] for more detail) . Furthermore, the volume change in the FREE (ΔV) can be determined based on Eq. 2.2 where V is the initial volume. Solving these three equations produces a map between the volume of fluid enclosed and

the FREE deformation.

$$\lambda_1^2 \cos^2\alpha + \lambda_2^2 \sin^2\alpha \left(\frac{(\theta+\delta)^2}{\theta^2}\right) = 1$$
$$\lambda_1^2 \cos^2\beta + \lambda_2^2 \sin^2\beta \left(\frac{(\phi+\delta)^2}{\phi^2}\right) = 1 \tag{2.1}$$
$$\frac{\Delta V}{V} = \lambda_2^2 \lambda_1 - 1 \tag{2.2}$$

Instantaneous Kinematics: FREEs deform upon actuation from pressurized fluids according to the governing equations in Eq. 2.1-2.2. Based on solving these equations for an infinitesimal volume change from the initial configuration, instantaneous deformation behavior can be mapped to the design space. Previous work [20] has shown motion patterns such as pure extension (along the upper AF line in Fig. 2.2) and contraction (lower AF line), axial rotation (along VF line) and more generally a screw motion or simultaneous translation and rotation. Furthermore, a unique one-dimensional manifold (known as the locked manifold LF in Fig. 2.2) which permits no increase in cylinder volume, and this resulting in no deformation is identified.

Configuration Memory Effect: Upon actuation by air (or liquid) pressure, the volume of the cylinder increases causing changes in its dimensions. This in turn changes fiber angles α and β. However, it was shown [20, 23] that the cylinder dimensions do not change once the deformed fiber orientations reached the locked manifold. Thus an initial configuration R of Fig. 2.2 terminates in a final locked configuration on locked manifold (LM). This effect, where every FREE with any initial fiber orientation always approaches a final orientation that belongs to the locked manifold is termed as "Configuration Memory Effect". Similarly Fig.2.2 also shows how upon increasing volume deforms FREEs, which start with fiber angles corresponding to Extension (E) and extension-rotation (S) approach their locked configuration. It is to be noted that FREE starting from S location extends and rotates till it reaches negative β fiber angle. From this point it contracts and rotates in opposite direction before it reaches its locked configuration. The FREE deformation

parameters can be estimated for a given pressure provided the material parameters are known beforehand. The next section details the design and construction of a soft helical manipulator with FREE as building block.

2.2 Design of spiral actuator

A detailed possibilities of adding single third fiber to the FREE structure has been explored in [19], where the helical actuators are obtained by selection of a base FREE from the workspace shown in Fig. 2.2 and adding a third fiber at an angle γ. Addition of third fiber adds an extra constraint due to which spatial motion is achieved. That is when a straight fiber is added, the extension is converted to bending due to this single fiber constraint. In this work we consider only third fiber with $\gamma = 0$ in order to ease the evaluation of curvature and torsion which will be used for the analysis proposed in Chapter 3. As the fiber selection is farther away from the $\beta = 0$ axis, the extension is more compared to the ones closer to the axis. This can be used to select the fiber angles based on size of cylinder to grasp. The larger the diameter of the grasping object, the β fiber should be larger to have a possibility of accomplishing the grasp.

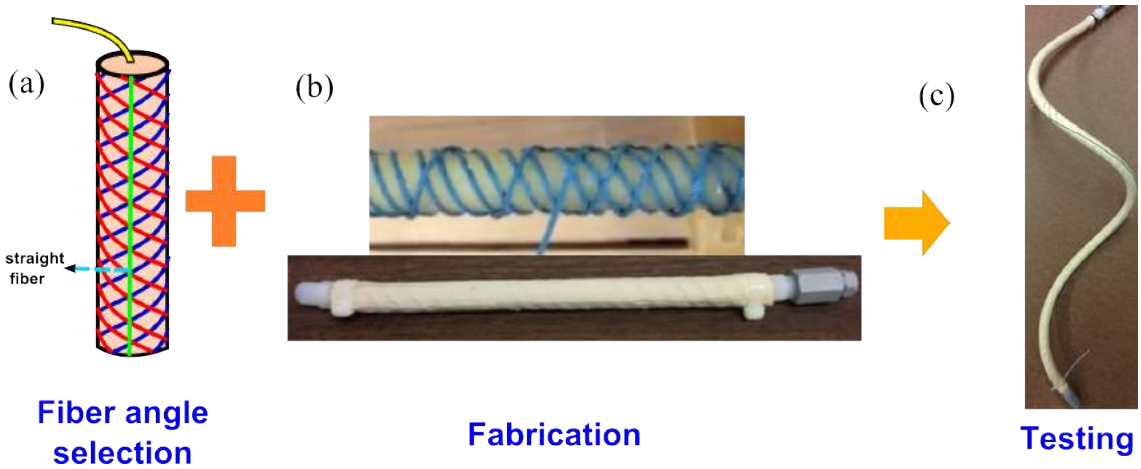

Figure 2.4: (a) Design selection from the FREE workspace, (b) Semi automated fabrication and (c) Testing

2.3 Fabrication

The construction of the FREE pneumatic actuators start with a base layer of natural rubber latex tubing with an inner diameter of 3/8 inch and 1/32 inch wall thickness(Kent Elastomer). Fibers are then wound in a semi automated fashion with the desired angle and orientation. Several adhesive agents are applied to cement the fibers on the latex. Finally, this matrix is coated with a layer of liquid elastomer and cured to obtain a composite structure as shown in Fig. 2.4 Finally a straight fiber is glued on this actuator in order to convert extension to bending and is tested for any failures.

3 GEOMETRIC EXACT MODELING

In this section, we present the framework for the analysis of the soft actuator, where we predict its final shape. Input pressure to the FREE actuators causes a change in its volume. This change in volume leads to changes in FREE length, diameter and leads to axial rotation and extension(the actuator can undergo contraction based on selection of the fiber angle) as detailed in Section.2.1. Based on the design of the manipulator elaborated in Section.2.2, any extension leads to bending or curvature in the actuator, while any axial rotation leads to torsion. Their combination leads to spatial deformation of the actuator, which will be evaluated using geometrically exact beam kinematics. The external forces including the self weight of the manipulator are also considered and the Cosserat beam mechanics [21] is solved to determine the exact deformed configuration. Cosserat beam theory has been to used to get the exact shape of other continuum actuators like OctArm [26], concentric tube manipulator [27] and other continuum robots [28] with accuracy less than 5% error which strengthens the use of Cosserat beam theory to get the exact shape of FREE based soft actuators.

3.1 Pressure to extension(λ_1) and rotation(δ) parameters

In Section **??**sec2:FREE we have detailed the relation between volume fraction change and the λ_1 and δ parameters. In this work we envision a pneumatic actuation to circumvent the change in the actuators weight with input volume change(we assume zero mass

to the input air). For simplicity, in this work the map between pressure and λ_1 and δ is experimentally obtained. A small length of the actuator is used to get its extension and rotation at different pressures as shown in Fig. 3.1 (a) and (b) in square dots and the experimental data is interpolated to get the parameters in the entire range.

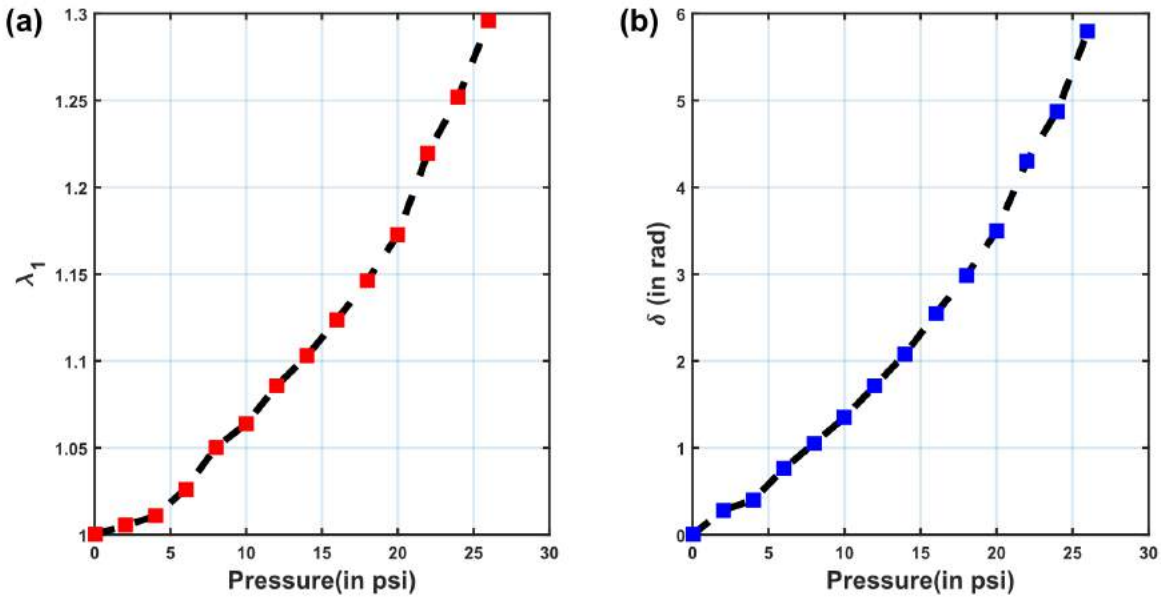

Figure 3.1: (a) Variation of λ_1 and (b) δ with pressure for FREE with $\alpha = 60$ degrees and $\beta = 88$ degrees.

3.2 λ_1, δ to curvature and torsion

As explained in Section2.2, the constraint posed by the straight fiber leads to constant curvature bending when the FREE extends. The curvature κ of the bend can be evaluated as in Fig . 3.2

$$\kappa = (\lambda_1 - 1)/2r \tag{3.1}$$

$$\tau = \delta/l \tag{3.2}$$

where r and l are the radius and length of the actuator.

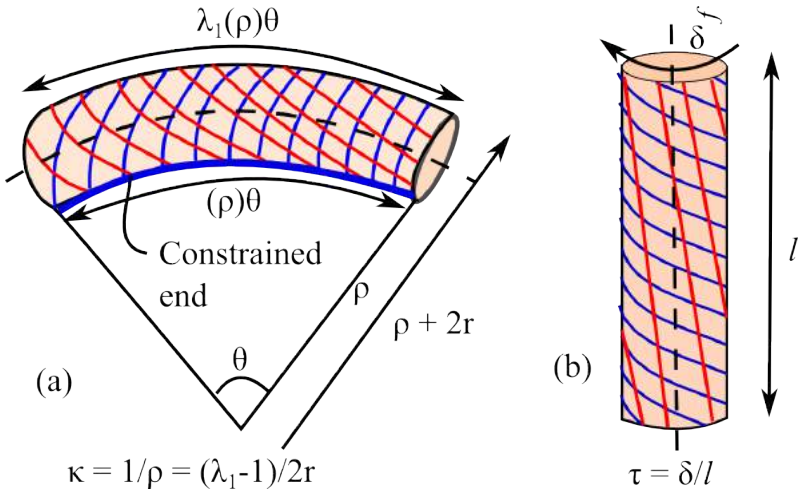

Figure 3.2: Estimation of curvature and torsion from λ_1 and δ

3.3 Spatial beam kinematics

In an ideal case i.e when there is no gravity, the torsion and curvature are constant throughout the length of the manipulator, leading to spatial helical motion. The manipulator shape can be characterized by its unstretched central axis curve as shown in Fig. 3.3.

The position of any point $s \in [0, L]$ on the curve is represented by $\mathbf{r}(s) \in \mathbb{R}^3$, a local frame (body frame) is defined which is at location s of the actuator. $\mathbf{R}(s) \in SO(3)$ is the rotation matrix which converts any vector in the local frame (body frame) to global frame . Suppose a vector $\mathbf{p}^l$ be position in local frame, a vector in local frame is denoted by a superscript l. The position $(\mathbf{p})$ in global frame is given by:

$$\mathbf{p} = \mathbf{R}\mathbf{p}^l \tag{3.3}$$

The variables $\mathbf{v}^l(s) = [v_1^l \; v_2^l \; v_3^l]^T$ and $\mathbf{u}^l(s) = [u_1^l \; u_2^l \; u_3^l]^T$ denote the linear and angular rates of change of $\mathbf{r}(s)$ and $\mathbf{R}(s)$ in the local frame, where v_1^l, v_2^l indicates the shear along local x and local y axes and v_3^l indicates the elongation or compression along the local z axis. Similarly u_1^l, u_2^l indicates the bending(curvature) about local x and y axes, u_3^l indicates the torsion about the local z axis. The following equations can be used to determine the final

shape of the actuator when there is no gravity:

$$\dot{\mathbf{r}}(s) = \mathbf{R}(s)\mathbf{v}^l(s)$$
$$\dot{\mathbf{R}}(s) = \mathbf{R}(s)\hat{\mathbf{u}}^l(s) \tag{3.4}$$

where $\hat{\mathbf{u}}^l$ indicates skew symmetric matrix of vector $\mathbf{u}^l$ [29].

$$\hat{\mathbf{u}}^{\mathbf{l}} = \begin{bmatrix} 0 & -u_3 & u_2 \\ u_3 & 0 & -u_1 \\ -u_2 & u_1 & 0 \end{bmatrix} \tag{3.5}$$

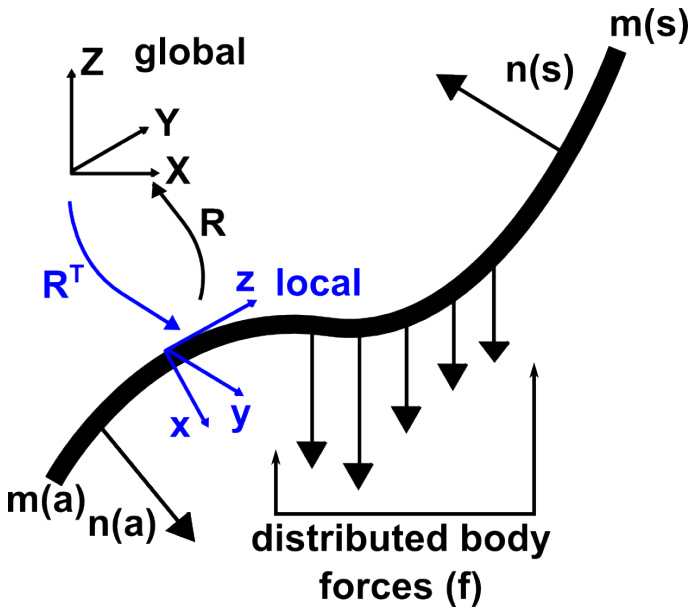

Figure 3.3: A section of the manipulator considered as a rod with the distributed forces, forces and moments

3.4 Cosserat rod mechanics

The previous section deals when there is no gravity and no other external forces acting on the actuator. But in reality there is gravity which activates the selfweight and also the end effector weight which needs to be considered in order to evaluate the exact shape of

the actuator. It has been reported that without the exact model of these soft actuators the model has close to 50% error in predicting the end position [26]. In order to estimate the forces by the actuator on the grasping object a more exact shape is needed which is our main objective in this work, thus necessitates the exact model in predicting the shape. The force and moment equilibrium for a section of the rod is given by:

$$\mathbf{n}(s) - \mathbf{n}(a) + \int_a^s \mathbf{f}(\varepsilon) d\varepsilon = 0 \tag{3.6}$$

$$\mathbf{m}(s) - \mathbf{m}(a) + \mathbf{r}(s) \times \mathbf{n}(s) - \mathbf{r}(a) \times \mathbf{n}(a) + \int_a^s (\mathbf{r}(\varepsilon) \times \mathbf{f}(\varepsilon) + \mathbf{l}(\varepsilon) d\varepsilon) = 0 \tag{3.7}$$

where $\mathbf{n}$ is the internal shear and axial forces (or stresses) $\mathbf{m}$ is the internal bending moment, $\mathbf{f}$ is the distributed self-weight per unit length. $\mathbf{l}$ is the body moment of the actuator. (Refer [27], [28] for details) It is to be noted that these equations are in global frame.On taking derivative of the equilibrium equations with respect to s we obtain:

$$\begin{aligned} \dot{\mathbf{n}}(s) + \mathbf{f_b}(s) + \mathbf{f_d}(s) &= 0 \\ \dot{\mathbf{m}}(s) + \dot{\mathbf{r}}(s) \times \mathbf{n}(s) + \mathbf{l}(s) &= 0 \end{aligned} \tag{3.8}$$

where $\mathbf{f}$ is composed of $\mathbf{f_b}$ and $\mathbf{f_d}$ which are the global distributed force due to body weight and other distributed forces acting on the section.

Linear constitutive equations are used to map the kinematic variables to the internal forces and moments [26].

$$\begin{aligned} \mathbf{n}(s) &= \mathbf{RD}(\mathbf{v}^l(s) - \mathbf{v}_0) \\ \mathbf{m}(\mathbf{s}) &= \mathbf{RC}(\mathbf{u}^l(s) - \mathbf{u}_0) \end{aligned} \tag{3.9}$$

where **C** and **D** are defined as:

$$\mathbf{C} = \begin{bmatrix} EI_1 & 0 & 0 \\ 0 & EI_2 & 0 \\ 0 & 0 & GJ \end{bmatrix} \tag{3.10}$$

$$\mathbf{D} = \begin{bmatrix} GA & 0 & 0 \\ 0 & GA & 0 \\ 0 & 0 & EA \end{bmatrix} \tag{3.11}$$

E, G are Youngs and Shear modulus, I, J and A are the second moment of inertia, polar moment of inertia and cross sectional area respectively.

Assuming zero body moments in our application, using Eq(3.4), (3.8),(3.9) we can arrive at the following system of equations:

$$\begin{aligned} \dot{\mathbf{r}}(s) &= \mathbf{R}(s)\mathbf{v}^l(s) \\ \dot{\mathbf{R}}(s) &= \mathbf{R}(s)\hat{\mathbf{u}}^l(s) \\ \dot{\mathbf{v}}^l(s) &= -\mathbf{D}^{-1}(\mathbf{R}^T\mathbf{f_b} + \hat{\mathbf{u}}^l\mathbf{D}(\mathbf{v}^l - \mathbf{v}_0) + \mathbf{R}^T\mathbf{f_d}) \\ \dot{\mathbf{u}}^l(s) &= \mathbf{C}^{-1}(-\hat{\mathbf{u}}\mathbf{C}(\mathbf{u}^l - \mathbf{u}_0) - \hat{\mathbf{v}^l}\mathbf{D}(\mathbf{v}^l - \mathbf{v}_0)) \end{aligned} \tag{3.12}$$

where $\mathbf{u}_0$ and $\mathbf{v}_0$ are the pre-curvatures and shears along the local axis. The body force $\mathbf{f_b} = \rho A g e_g$, where ρA is mass per unit length, g is acceleration due to gravity , $\mathbf{e}_g$ is direction of gravity.

3.5 Boundary conditions

From the force balance equation for the entire length of the manipulator we have:

$$\mathbf{n}(L) - \mathbf{n}(0) + \int_0^L (\mathbf{f_b}(\varepsilon) + \mathbf{f_s}(\varepsilon) d\varepsilon) = 0 \tag{3.13}$$

the force at $\mathbf{s} = \mathbf{L}$ is the end cap weight which is $\mathbf{EC_f}$ and body force $\mathbf{f_b}$ integrated over the entire length is the weight of the actuator (which is $\rho AgL * e_g$). Plugging in this known parameters into the Eq.3.13 we obtain the boundary condition for $\mathbf{v^l}(s = 0)$:

$$\mathbf{v^l}(s = 0) = \mathbf{D^{-1}}(\mathbf{EC_f} + \rho \mathbf{Age_g L} + \int_{\mathbf{0}}^{\mathbf{L}} (\mathbf{f_d}(\varepsilon) \mathbf{d}\varepsilon)) \tag{3.14}$$

The boundary condition for $\mathbf{u^l}(s = L)$ should be the pre-curvatures ($\mathbf{u_0}$) , $\mathbf{r}(s = 0) = [0\ 0\ 0]^T$ and $\mathbf{R}(s = 0)$ is identity matrix.

With these boundary conditions and the system of equations Eq.3.12, the positions, Rotation, curvatures and shears can be obtained for the entire length of the actuator. Matlab bvp4c command is used to obtain the solution in this work. For getting the exact shape of the spiral actuator when actuated to a certain pressure, in the initial conditions for $\mathbf{v^l}(s = 0)$, $\mathbf{f_d}$ is set to zero as there is no external distributed force acting on the actuator other than the body force.

4 FORCE ESTIMATION OF SPIRAL ACTUATOR

Upon actuation to a given pressure, the spiral actuator deforms to its exact shape which can be predicted by the Cosserat model presented in the previous chapter. In order to further deform its current deformed shape obtained by actuation, there needs to be either an external force or moment to be acted on the deformed spiral actuator. For the task of grasping a cylindrical object as shown in Fig.4.1, the cylindrical object acts as a constrain for the spiral actuator to get to its exact shape. In this particular case there are forces(f_{di}) acting on the actuator due to its contact with cylinder which deforms spiral actuator's shape.

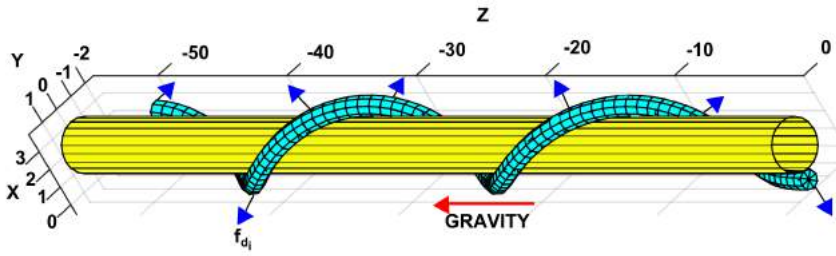

Figure 4.1: The object acts as a constrain for the actuator to go to its exact shape, thus a normal force is exerted by the cylinder on the spiral actuator. f_{di} is the distributed force acting on the actuator by the cylinder

In this chapter an algorithm is presented in order to get an estimate of the normal force exerted on the spiral actuator due to its contact with the cylindrical object. Figure 4.2 shows the overall process involved starting from estimating curvature, torsion and getting the exact shape of the spiral actuator which have been thoroughly presented in the previous chapter. In order to estimate the forces, information about the location of cylinder is desired and then the forces are estimated based on the contact between the

cylindrical object and the spiral actuator.

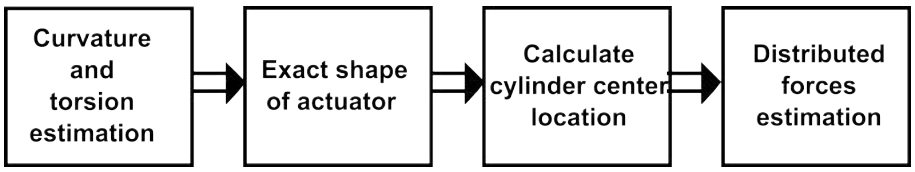

Figure 4.2: The steps needed to estimate the distributed forces

4.1 Cylinder center calculation

Let the cylinder center be given by $C_c = [x_c, y_c]$ where x_c, y_c are x and y coordinates of the center. It is assumed that the radius of the cylinder R_c is known beforehand. For a given pressure (i.e curvature and torsion) the exact shape of the spiral actuator $r_0(s) \in R^3, s = [0 : L/n_t : L]$ is known where n_t is the number of points the entire length is discretized into. The initial point (or section) of the spiral($r_0(s = 0)$) should lie on the circumference of cylinder and having the actuator in the center of the cylinder is preferred in order to have a uniform force distribution. The above criterion can be satisfied by solving the below optimization routine

$$\underset{x_c, y_c}{\text{minimize}}\ w_1.P + w_2.Q$$

where P is the planar distance between the initial point (or section) and the cylinders circumference and Q is the distance between the cylinder center and actuators exact center which is average of the x and y coordinates of the actuator shape. w_1 and w_2 are the weights in order to make both the criterion of the same order.

4.2 Distributed forces estimation

Once the information of the cylinder center and the exact shape of the spiral are known, distributed forces acting (f_d) are to be estimated. In order to make the algorithm efficient

the overall nonlinear problem is solved as a quasilinear problem. The following algorithm shown in Fig.4.3 is proposed which will be explained in this section:

4.2.1 Inputs and initialization

The force estimation starts off with prior information of the following parameters:

r_0 : [x,y,z] at n_t points

C_c : Center of cylinder $[x_c, y_c, 0]$

R_c : Radius of cylinder

np_f : No. of points force is applied

n_b : No of points expected to be in contact with cylinder circumference

n_t : Total no of points the length is discretized into
and we initialize $step = 1$ and $iter = 1$.

4.2.2 Sensitivity matrix calculation

Next the sensitivity is calculated, that is to calculate the displacements of n_t points of the actuator when a unit force (f_0) is applied first in global x direction at np_f points and then in global y direction at np_f points.

$$\Delta r_i^{step} = r_{0i} - r_0 \tag{4.1}$$

where r_{0i} is the new position of the actuator with force f_0 applied in global x direction $\forall i = [1, \ldots, np_f]$ and in global y direction $\forall i = [np_f, \ldots, 2np_f]$. It is to be noted that np_f are the positions corresponding to the length divided into np_f points.
This is solved by solving Eq.3.12 obtained in previous chapter $2np_f$ times.

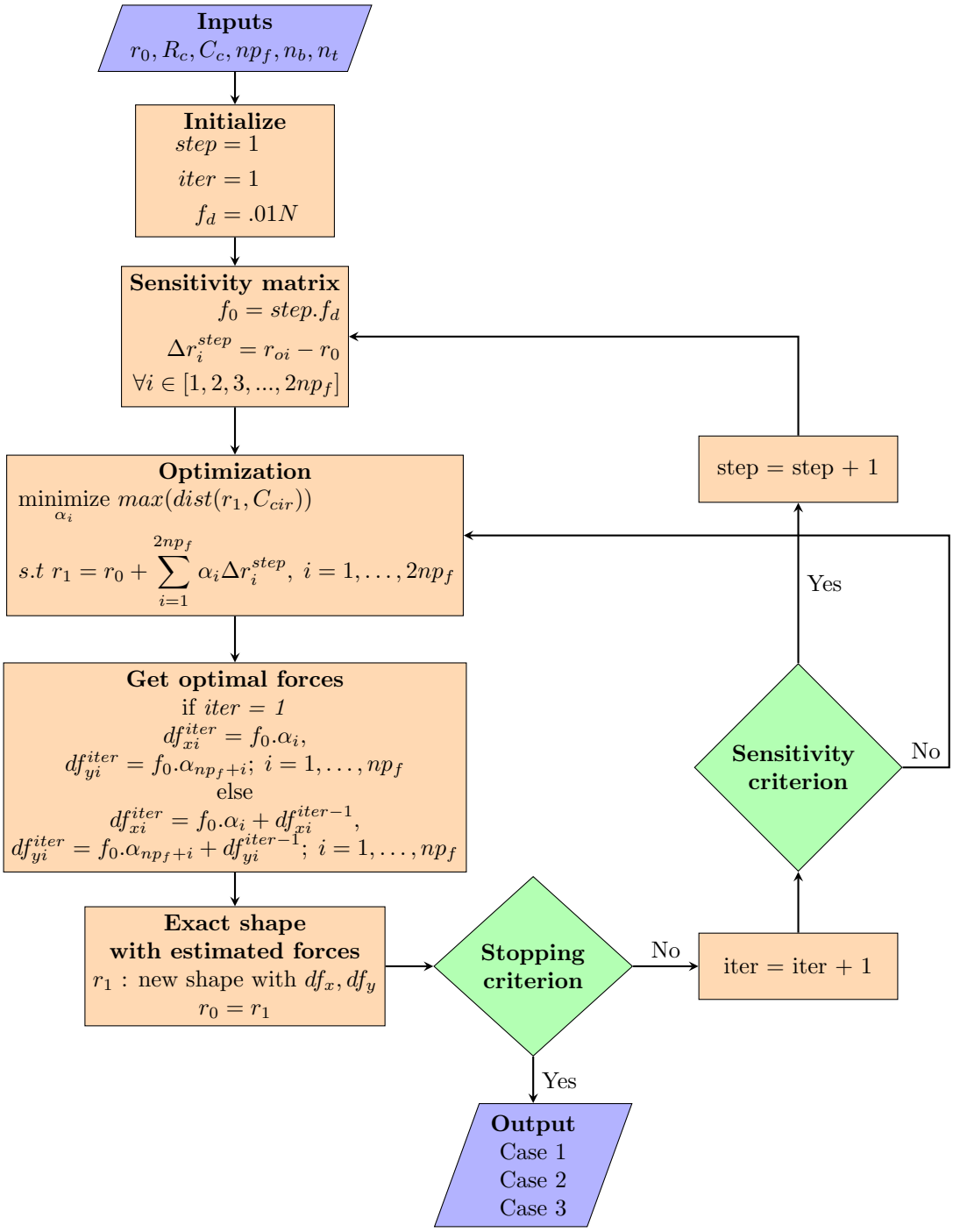

Figure 4.3: Flowchart to estimate the distributed forces acting on the spiral actuator

4.2.3 Optimization for force variables

Next the force variables$(\alpha_i's)$ are solved using optimization. Here the force variables are calculated in order to minimize the maximum distance of new deformed shape (r_1) and the cylinder's circumference (C_{cir}). The distance between any discretized point on the actuator r_1 and the cylinder circumference is evaluated in the direction of vector pointing from cylinder center to the particular point on r_1 as shown in Fig.4.4. The optimization is done for the specified n_b discrete points.

$$\begin{aligned} &\underset{\alpha_i}{\text{minimize}} \quad max(dist(r_1, C_{cir})) \\ &s.t \quad r_1 = r_0 + \sum_{i=1}^{2np_f} \alpha_i \Delta r_i^{step},\ i = 1, \ldots, 2np_f \end{aligned} \tag{4.2}$$

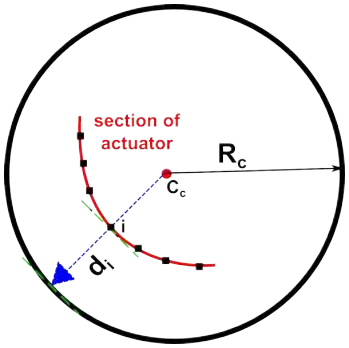

Figure 4.4: Distance between discretized points (in black squares) and cylinder circumference is measured in the direction of vector from center to the discretized point (i) on the section of the actuator

4.2.4 Optimal forces and updated exact shape

Once the force variables are evaluated, the forces needed to conform to cylinder are solved for. The distributed forces are product of the obtained force variables and the epsilon force applied f_0 for the first iteration. For the next iterations it would be the sum of forces obtained in previous and the current iteration because this iteration force is applied on the deformed shape obtained in the previous iteration. The distributed force update is given

as:

$$\text{for } i = 1,2,\ldots,np_f \tag{4.3}$$

$$\begin{aligned} df_{xi}^{iter} &= f_0.\alpha_i & df_{yi}^{iter} &= f_0.\alpha_{np_f+i} & &\text{if iter = 1} \\ df_{xi}^{iter} &= f_0.\alpha_i + df_{xi}^{iter-1} & df_{yi}^{iter} &= f_0.\alpha_{np_f+i} + df_{yi}^{iter-1} & &\text{if iter} > 1 \end{aligned}$$

It is to be noted that the current r_1 is not the final exact shape obtained with these forces as this is obtained by considering it as a linear system. In order to get the exact shape(r_1) the set of equations Eq.3.12 are solved with the obtained distributed forces. The r_0 is updated to r_1 for the next iteration.

4.2.5 Stopping criterion

When the final shape r_1 conforms to cylinder circumference the objective is reached. In order to check this occurrence a stopping criterion is framed which calculates the average XY planar distance between cylinder center C_c and the final shape r_1 for n_b points ($mean_{dist}$). The criteria is set to the absolute difference between the $mean_{dist}$ calculated and radius of cylindrical object R_c.

$$criteria_{iter} = |mean_{dist} - R_c|$$

The iterations are stopped if the following stopping criterion is met:

$$criteria_{iter} < \varepsilon_1 \qquad \text{for } iter = [1,2,3] \tag{4.4}$$

$$|criteria_{(iter-3)} - criterai_{iter}| < \varepsilon_2 \qquad \text{for } iter > 3 \tag{4.5}$$

ε_1 and ε_2 are chosen such that $\varepsilon_2 < \varepsilon_1$. If there is no substantial change in the criteria over three iterations, the process is terminated. This condition takes care of cases when it is

stuck at a particular shape before satisfying a strict bound ε_1.

4.2.6 Sensitivity calculation criterion

In the case when stopping criterion is not satisfied, then there are two ways the algorithm can proceed. The first way is to do optimization of forces on the new shape (r_1) with the previous calculated sensitivity matrix and other option is to recalculate the sensitivity matrix. As the algorithm is solved with a linear assumption, there are bounds on $\alpha_i's$ which restricts the search space to this bounded region. So in order to reach its true optimal solution with the current sensitivity matrix, it may have to do more iterations on the updated shape (r_1). In this case the former one is preferred. There is a possibility that with the applied force the change is relatively less, in these cases the convergence of the algorithm will improve if sensitivity is calculated for a higher force, under such circumstances second option is preferred.

The following condition when satisfied proceeds with the calculation of new sensitivity matrix:

$$\left|\frac{criteria_{(iter-3)}}{criteria_{iter}}\right| < \varepsilon_3 \qquad \text{for } iter > 3 \tag{4.6}$$

ε_3 is chosen which is sightly greater than 1.

4.2.7 Outputs

When the stopping criterion is satisfied. The outputs of the final shape r_1 and the distributed forces df_x and df_y and the $criteria_{iter}$ are obtained. From the distributed forces the normal force which is the component of force radially pointing outwards is calculated along the length of the curve. The overall normal force can be found by integrating the distributed force about the length of the actuator.

Based on these outputs, there are three possible cases listed below:

- **Case 1: Criteria satisfied and positive normal force profile**

  When the *criteria* is less than the desired threshold and has a consistent positive normal force profile throughout implies a perfect desired wrap. From the positive normal force profile it can be concluded that the entire length of the actuator is used in the wrap which is plausible.

- **Case 2: Criteria satisfied and partial negative normal force profile**

  When the *criteria* is less than threshold but some regions of negative normal force along the length are observed, it can be concluded that such a case is not possible as there is no external force or contact which will apply force on the actuator in direction pointing radially inwards.

- **Case 3: Criteria not satisfied**

  In this case when the *criteria* is not satisfied implies that there is no possibility of conforming to the given cylinder of radius R_c with the given initial shape r_0 using its entire length.

4.3 Classification of spiral actuator gripping

It is observed that there are three phases as a sweep of pressure is done on a given cylindrical object which are termed as:

- Overhang region :

  This occurs at low pressures before it reaches a state where the entire actuator is in contact with the circumference of the cylinder. So it turns out that there are only distributed forces on the actuator only till the point of contact. It is to be noted that the distributed forces due to the manipulator weight are always present, we are focusing on the radial distributed forces which deform the true exact shape of the spiral actuator at a given pressure.

This can be related to Case 2 where there are negative forces in some regions of the actuator.

- Perfect wrap region:

  This is the region where the entire actuator is in contact with the the circumference of the cylinder which in turn implies there are distributed forces acting throughout the actuators length to constrain the position to the circumference of the cylinder.

  This can be related to Case 1 where the entire length is used for wrap and has positive normal force profile.

- End curl region:

  If the actuation pressure is gradually increased from the perfect wrap region, it is observed that at the end the spiral actuator unwraps itself from the cylinder in order to get to its initial shape. In this case there are forces throughout because there are still some points which are in contact with the cylinders circumference. But portion of end section is not exactly conforming to the cylinders circumference.

  This can be related to case 3 where there isn't a chance for using the entire length to wrap the given cylindrical object.

The overhang and end curl cases are shown in Fig.4.5.

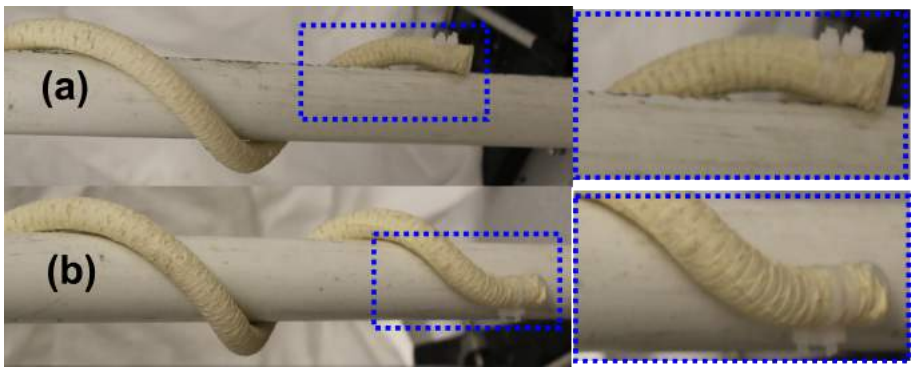

Figure 4.5: (a) Over hang region when conforming to a cylinder (last section is not in contact with the circumference) and (b) End curl region when the last section is starting to unwrap.

4.4 Modifications in algorithm

In this section an intuitive modification in the algorithm are presented to solve for the Case 2 and Case 3. This changes assist in predicting the overall shape and normal forces when these scenarios occur.

- Case 2 : When there is a negative normal force profile, it indicates that in real scenario some end section of the spiral actuator is not in contact with the cylinder circumference and is overhanging. This is taken care by forcing the force on end sections of the actuators to zero. As shown in the Fig.4.6 there are $np_f - 1$ number of sections when force is acting on np_f points. In the Fig. 4.6 the entire length of the actuator is discretized to n_t points. So iteratively force in global x and y direction starting from np_f are set to zero and the optimization routine tries to estimate forces to conform the actuator only to the length on which there is force acting. For example if np_f is set to zero then n_b(number of points which the optimization routine tries to conform to the cylinder) is set to $n_t - ceil(n_t/np_f)$. This continues till there is no negative force profile.

Figure 4.6: Discretization and forces acting for sensitivity calculation

- Case 3: In this case the last section curls thus a section of length doesn't conform to cylinder but there is force acting on it to keep the last section outside cylinders circumference. This is solved by the above algorithm by careful choice of the portion of the actuator confirming to the cylinder (n_b). Note that the forces are still acting in all the $np_f - 1$ sections.

5 RESULTS

In this chapter the first section presents the experiments conducted to get the pressure versus extension and pressure versus rotation mapping, followed by method to estimate Youngs modulus and then using these experimental values modeling results are presented in the second section. In this chapter the modeling is conducted on the data obtained from a single prototype with the following parameters : $\alpha = 88$ degrees, $\beta = 60$ degrees, L = $.57m$ and mass per unit length = $.0441kg/m$.

5.1 Pressure vs λ_1, Pressure vs δ mapping

In order to obtain the exact shape and/or to obtain the distributed normal forces proposed in Chapter 3 and Chapter 4, curvature and torsion at given pressure are to be known beforehand. In Chapter 3 the method to obtain the curvature and torsion is presented provided that the extension(λ_1) and rotation (δ) parameters are known. Here experimental method used to obtain λ_1 and δ with varying pressure is detailed.

A specimen which is a section of the fabricated actuator of length 10 cm is used. This

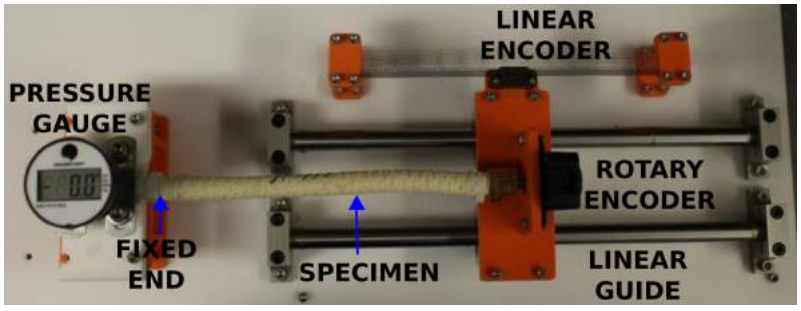

Figure 5.1: Experimental setup to get Pressure vs Extension(λ_1) and Pressure vs Rotation(δ) mapping

section is snipped before winding the straight fiber to the fabricated actuator for use in this experiment. The experimental setup is shown in Fig.5.1 where one end of the specimen is fixed and other end of the specimen is allowed to extend and rotate without any constraint. The linear encoder (US Digital EM1-0-250-N, US Digital LIN-250-6-N, 250 counts per inch) and rotary encoder (US Digital H5-1250-NE-S, 1250 counts/revolution) are used to measure the linear and rotational displacements for a given pressure. The entire map is obtained by varying the input pressure to the specimen from 0 psi to 24 psi (in steps of 2 psi) and by recording the corresponding extension and rotation from the encoders. Fig.3.1 shows the map obtained from this experiment.

5.2 Youngs modulus estimation

Soft actuators are primarily composed of materials which have less Young's modulus which enhances their compliance under loading [30]. Pneumatic actuators like the FREE considered in this work has variation in their Youngs modulus with varying pressure. FREEs are composites of a base elastomer and fibers wound at chosen angles. This composition of fibers also contributes in variation of Youngs modulus. Hence an experimental method is presented here in order to estimate the Youngs modulus of FREE with given fiber angles α and β.

Figure.5.2 shows the experimental setup to record the deflection of the specimen at different pressures when gravity is acting downwards. The deflection occurs due to the self weight of the specimen and the weight of end cap. With the knowledge of the length of the specimen at different pressures, weight of the specimen and the end cap, at a given pressure, the following optimization problem is solved to estimate the Youngs modulus .

$$\underset{E_a}{\text{minimize}} \; ((x_e - x_a)^2 + (y_e - y_a)^2)^{1/2}$$

where $[x_e, y_e]$ are the x, y coordinates of the end point obtained from experiments and $[x_a, y_a]$ are the x, y coordinates of the end point from FEA at a given pressure and E_a is the Youngs modulus variable in the Finite Element Analysis. For the given prototype the variation of Youngs modulus is less than 7% therefore the average of the Youngs modulus which is $7e5N/m^2$ is the value considered for the prototype in this modeling.

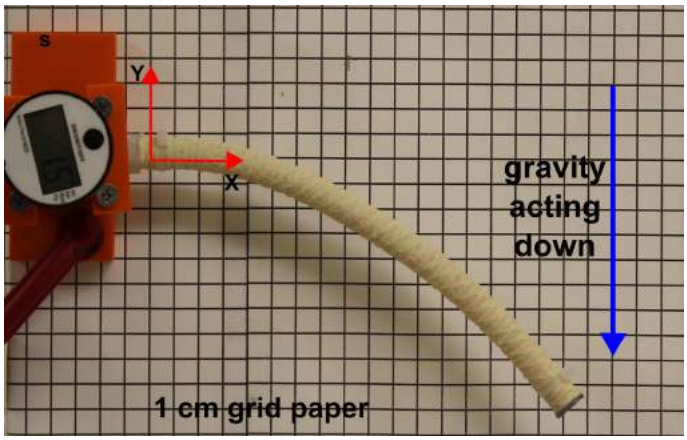

Figure 5.2: Experimental setup for estimation of Youngs modulus (E)

5.3 Modeling results

In this section with the information of experimental values of Youngs modulus(E) and the mapping of P vs λ_1 and δ, the results of modeling detailed in Chapter 3 for obtaining the geometric exact shape and Chapter 4 for estimation of the normal forces are presented respectively.

5.3.1 Exact shape of spiral actuator

Figure 5.3 shows the spiral actuator actuated from 12 psi to 20 psi in steps of 2 psi when there is no gravity (that is no self weight and end effector weight). It can be observed from the Figures that they have a constant curvature and torsion thus leading to a helix at different actuation pressures. But as detailed in Chapter 3, soft actuators unlike rigid

robots deform due to self weight and other forces acting on them due to their intrinsic compliance. Figure 5.4 shows the shape obtained using the geometric exact model. Here it can be observed that due to its self weight and end cap weight the actuator is closer to the Z axis. The difference observed between the exact model and non exact model is significant when long actuators are considered (as in this case).

In order to confirm that the exact shape is not a helix, Fig.5.5 is presented which is the top view of the actuator when actuated to 20 psi. For a helix, the axial top view will be a circle.

5.3.2 Distributed force estimation

The results obtained from Chapter 4 are presented here when a cylindrical object with diameter $R_c = 13.5$mm is the object of interest for grasping.

(a) Pressure = 10 psi, $\mathbf{n_t} = 101$, $\mathbf{np_f} = 20$ and $\mathbf{n_b} = 101$

Figure.5.6 shows the top view (5.6(a)) and 3D view (5.6(b)) with azimuth = 35 degrees and elevation = 80 degrees. A perfect wrap is obtained as the algorithm optimizes for forces to wrap the entire length of the actuator $(n_b = n_t)$. But it can be observed that there is negative force profile from the normal force profile shown in Fig.5.6(c). The negative force is after 50% of length of the actuator which implies the situation in Case 2, where a radially inward force is applied to wrap the actuator to cylinder.

Considering that with $np_f = 20$ and $n_b = 101$ Case 2 scenario is obtained, simulations are run with the modifications in algorithm when Case 2 is detected. For simulations with the following parameters $[np_f, n_b] = [19, 95]$ negative force profile in the later sections of the actuator is detected.

(b) Pressure = 10 psi, $\mathbf{n_t} = 101, \mathbf{np_f} = 17$ and $\mathbf{n_b} = 85$

For these parameters at 10 psi a positive force profile across the entire length of the actuator is detected as shown in Fig.5.7(c). The top view and 3D views are shown in Fig.5.7(a) and Fig.5.7(b). The red arrow in the 3D view points to the hanging section. There is a

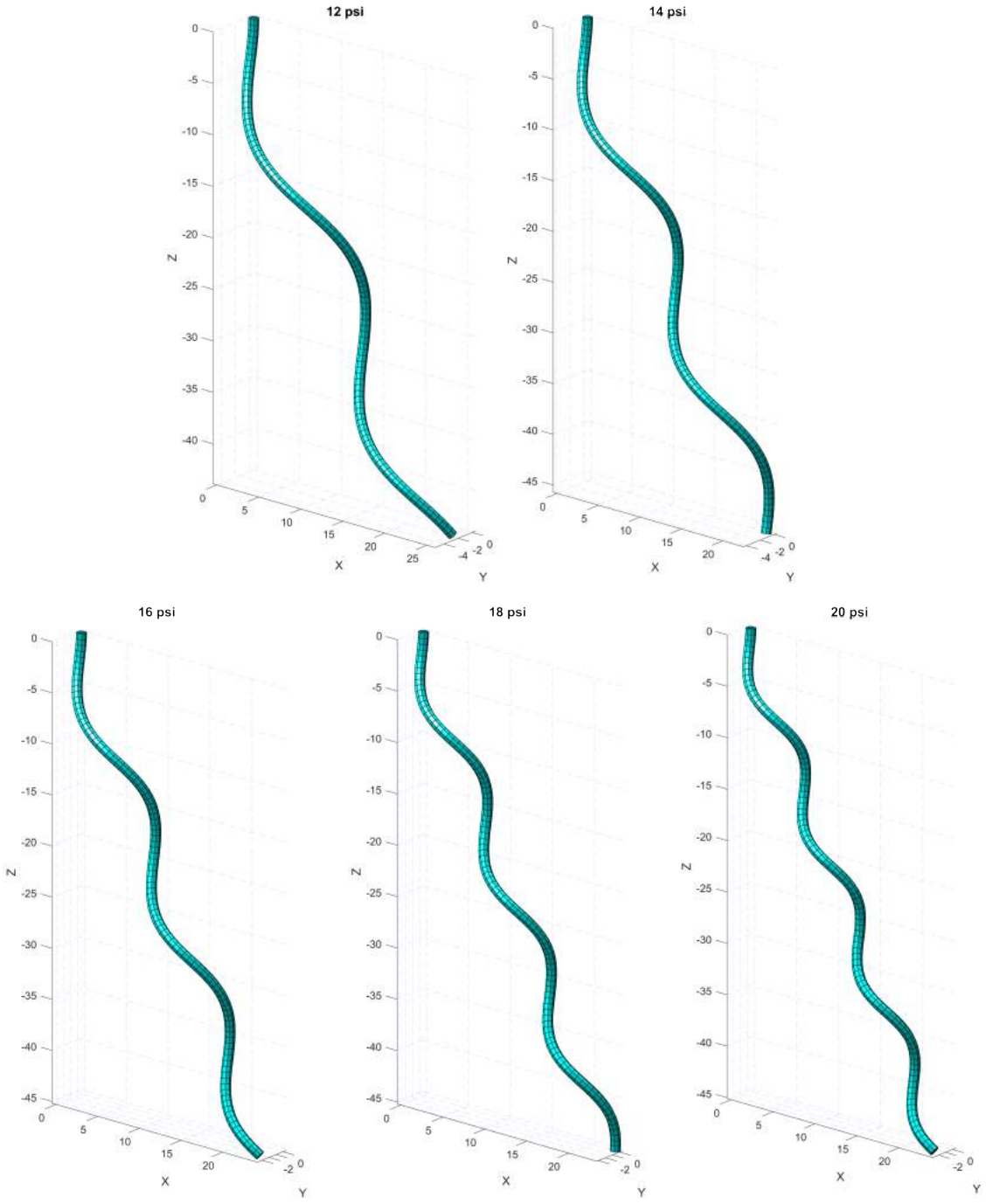

Figure 5.3: Shape of the spiral actuator actuated from 12 psi to 20 psi in steps of 2 psi. Gravity is not considered thus leading to a helical final shape.(All axes are in cm)

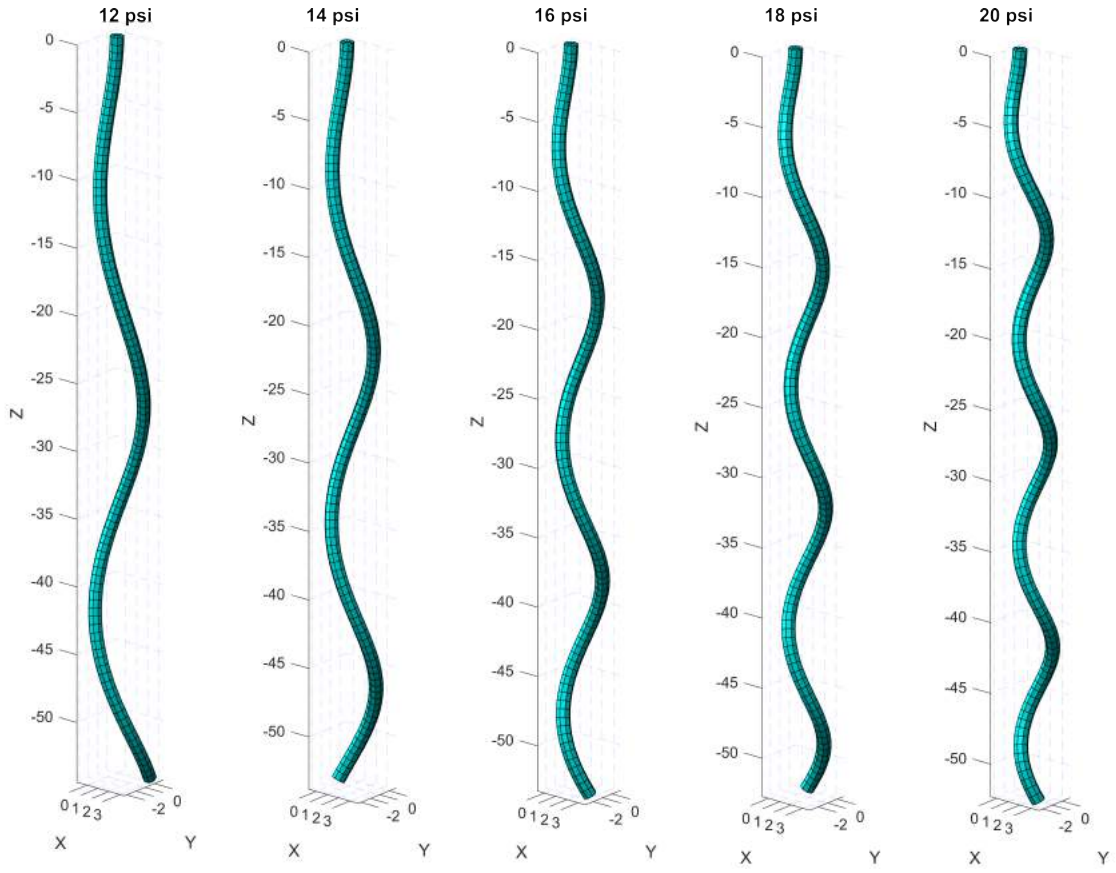

Figure 5.4: Final exact shape of the spiral actuator actuated to 12 psi to 20 psi in steps of 2 psi. Due to gravity the shape is closer to Z axis.(All axes are in cm)

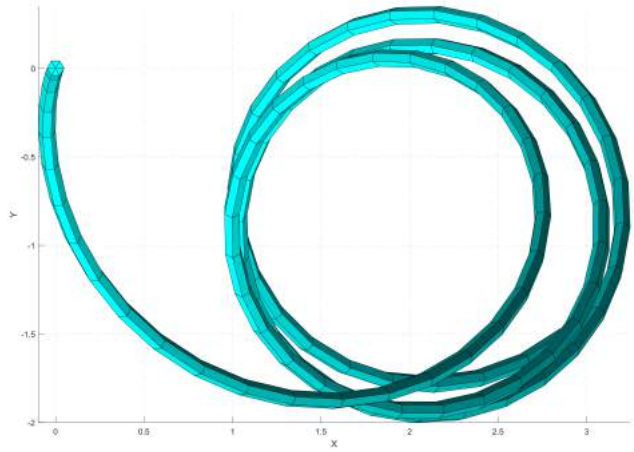

Figure 5.5: Top view of exact final shape of the spiral actuator actuated to 20 psi.(All axes are in cm)

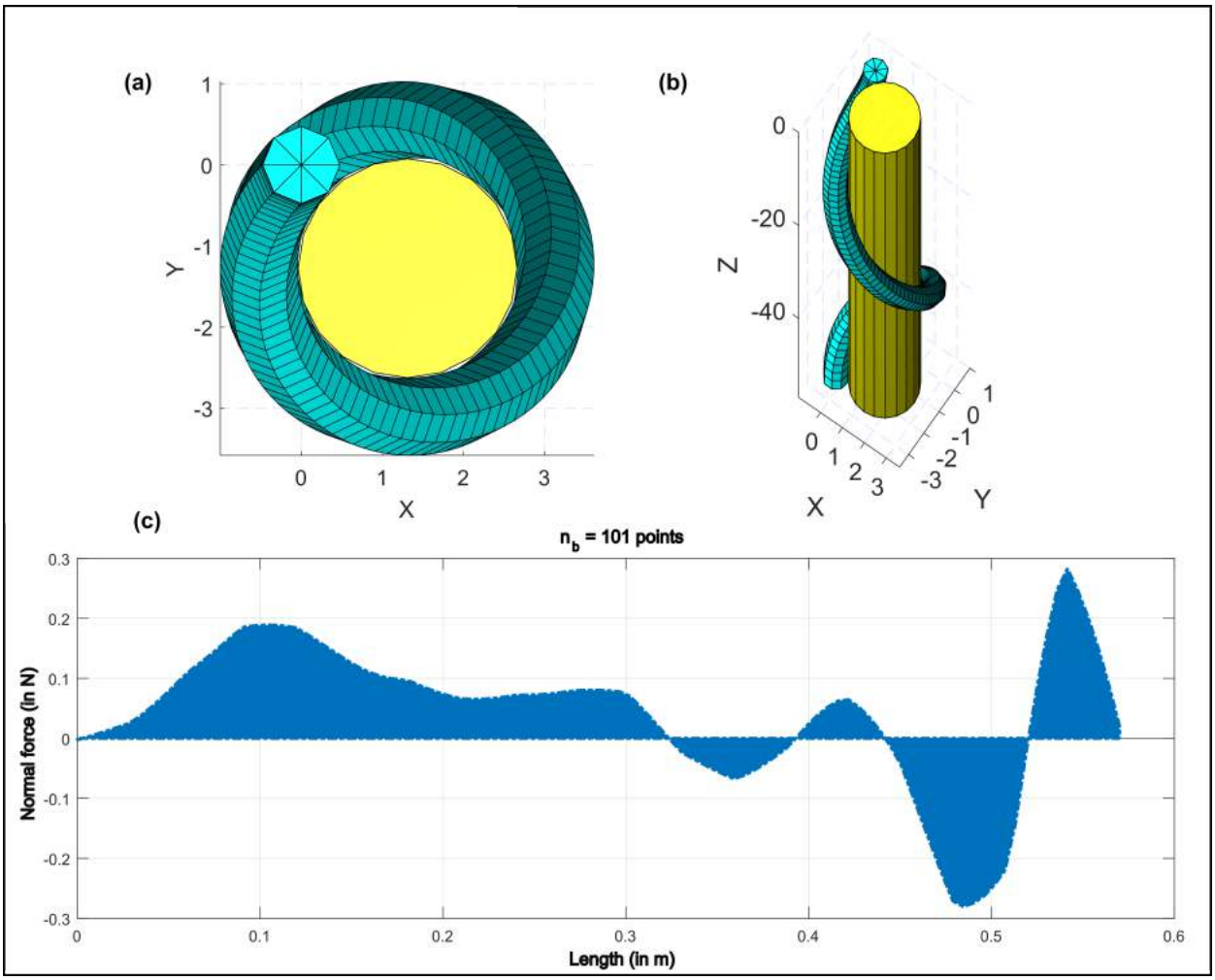

Figure 5.6: (a)Top view with cylindrical object (in yellow) when actuated to 10 psi with n_b = 100 points (b) View with az = 35deg. and al = 80 deg. where a perfect wrap is obtained (All axes are in cm) but (c) The normal force along the length of the actuator has negative force after 5% of actuator's length thus indicating Case 2.

negative force in the initial 5% length of the actuator, this occurs due to the position error of the cylinder center calculated by optimization. Due to this error the circumference of the cylinder is not exactly tangential to the actuators deformed shape in the initial section and hence a negative force obtained in this initial region.

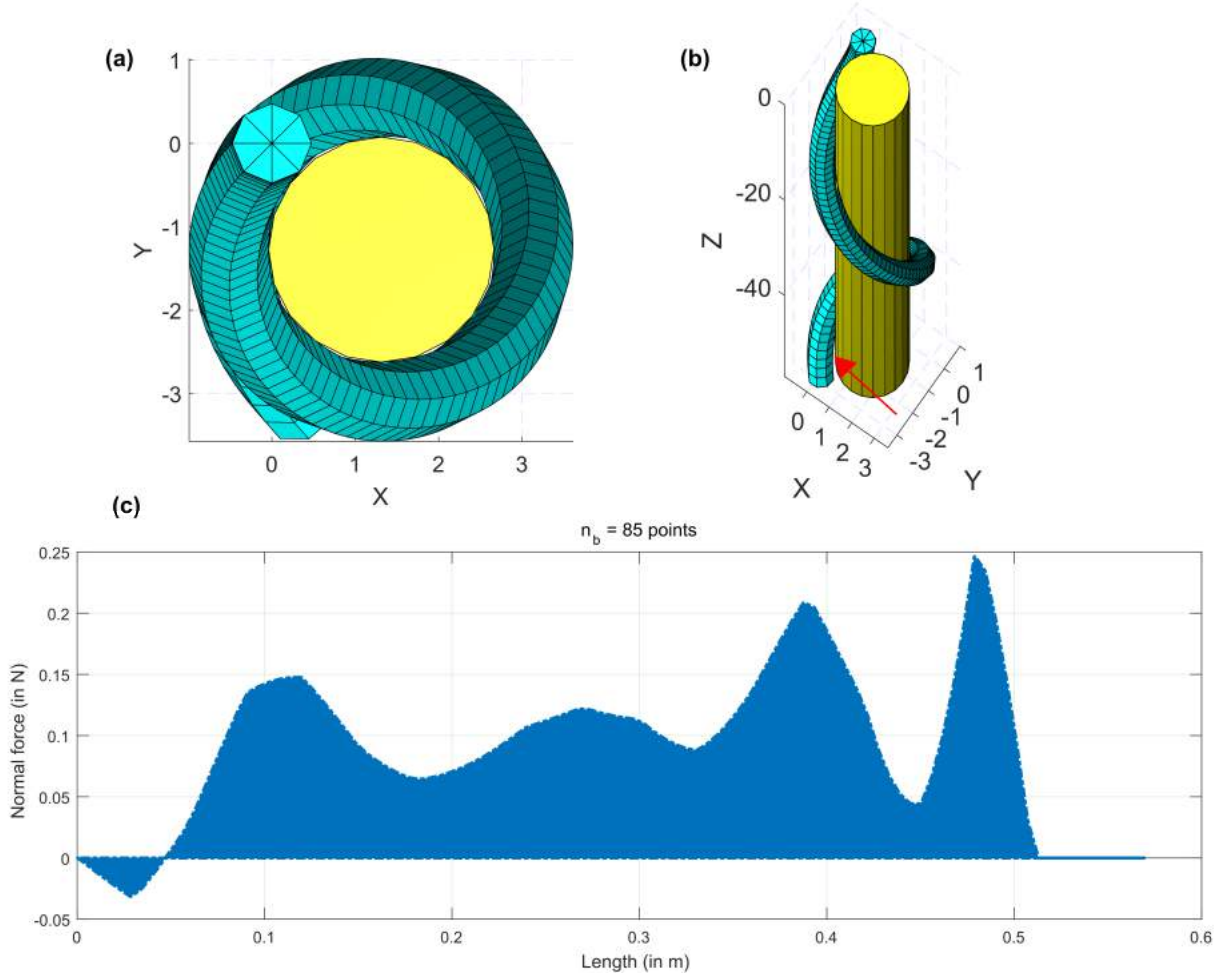

Figure 5.7: (a)Top view with cylindrical object (in yellow) when actuated to 10 psi with n_b = 85 points (b) View with az = 35deg. and el = 80 deg. where the arrow points to the hanging section (All axes are in cm) and (c) The normal force along the length of the actuator, no negative force after 5% of actuator's length.

(c) Pressure = 12 psi, $\mathbf{n_t = 101, np_f = 18}$ and $\mathbf{n_b = 90}$

Next the modeling results obtained for 12 psi with $np_f = 18$ and $n_b = 90$ are shown in Fig.5.8. Similar to the previous instance at 10 psi a negative force profile was obtained with $[np_f, n_b] = [20, 101]$ and $[19, 95]$. Fig.5.8(b) shows the hanging section. A negative

force profile is observed in the initial section (see5.8(c)) of the actuator even in this case which is due to the starting section not been perfectly tangential to cylinders circumference.

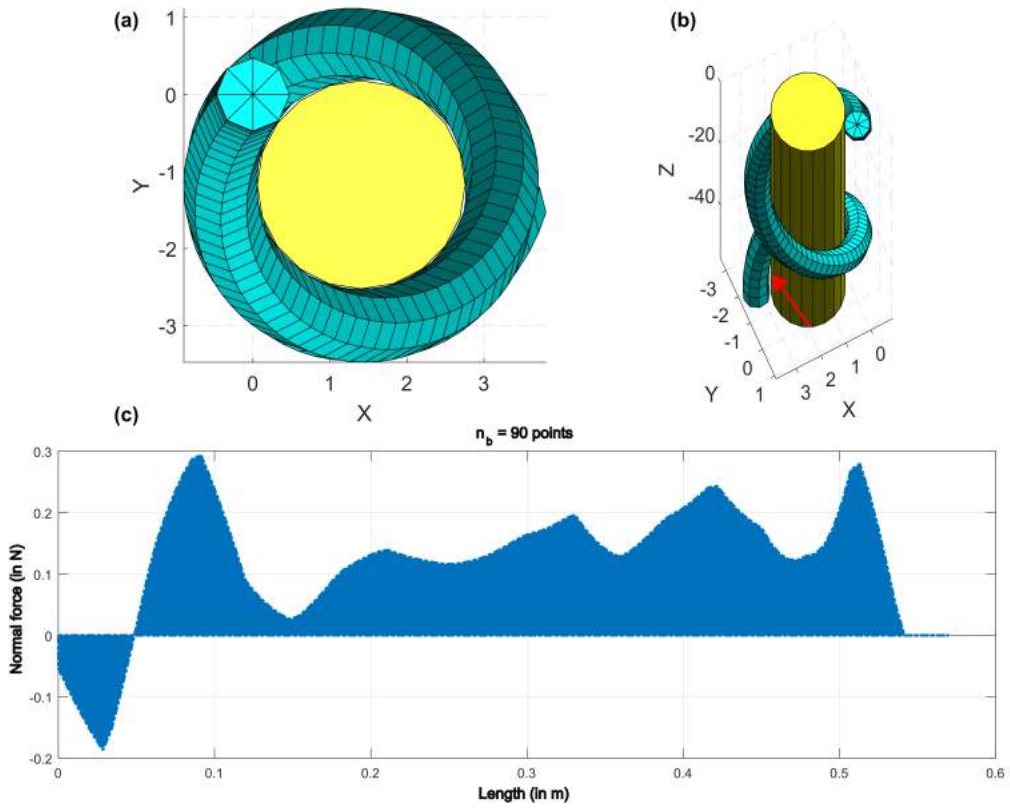

Figure 5.8: (a)Top view with cylindrical object (in yellow) when actuated to 12 psi with n_b = 90 points (b) View with az = 154 deg and el = 180 deg where a perfect wrap is obtained (All axes are in cm) and (c) The normal force along the length of the actuator has no negative force after 5% of actuator's length

(d) Pressure = 16 psi, $\mathbf{n_t = 101, np_f = 20}$ and $\mathbf{n_b = 101}$

For 14 psi, 16 psi and 18 psi the simulation results give a perfect wrap with positive force profile, thus indicating Case 1 where the entire actuator is used for grasping. When the model is run for curvature and torsion values at 16 psi, the following results shown in Fig.5.9 are obtained. Fig. 5.9(a) and (b) shows the top and 3D view(with az = -90 and el = 60), here it can be observed that there is no hanging section at the end of the actuator and moreover in Fig.5.9(c) a positive force profile throughout confirms Case 1 scenario

for this pressure

Variation of total force with varying pressure

When the spiral actuator is actuated from low pressures to higher pressures, the actuator final shape gets closer to its central axis. In the scenario when the actuator is given a cylindrical object to grasp, more distributed normal force is needed at higher pressures to keep the actuator conformed to the cylinder. As at higher pressures the distance between actuator and cylinder circumference increases thus more force is needed for deformation. The following Fig.5.10 shows the variation in force with increasing pressure when pressure is varied from 10 psi to 18 psi in grasping a cylindrical object with $R_c = 13.5$ mm. The force increases with increase in pressure. It is to be noted that at 10 psi and 12 psi the forces are when only 85% and 90% of the actuators length is used for grasping (Case 2).

Choice of np_f

In the proposed algorithm there is an important parameter selection of the number of points the force is applied for sensitivity calculation (np_f). This dictates the computational time, larger the choice ($<= 100$), the more time it takes as it needs to solve the system of equations Eq 3.12 for (2*np_f) times. Twice because a delta force is applied in X and Y direction at each point. More number of points assists in achieving more accurate force estimation as it is close to ideal where no interpolation is used (if np_f = 101). Figure.5.11(a) and (b) shows the variation in the total normal force for increasing number of np_f. Fig.5.11 (a) is the total normal force obtained at 16 psi for a cylindrical object with $R_c = 13.5mm$ for increasing np_f and Fig.5.11.(b) is the total normal force obtained at 12 psi for cylindrical object with $R_c = 21mm$ for increasing np_f. In this work $np_f = 20$ is selected whose total normal force is close to the mean of the normal forces obtained at different np_f. This selection also is twice as quick when compared to the selection of $np_f = 40$.

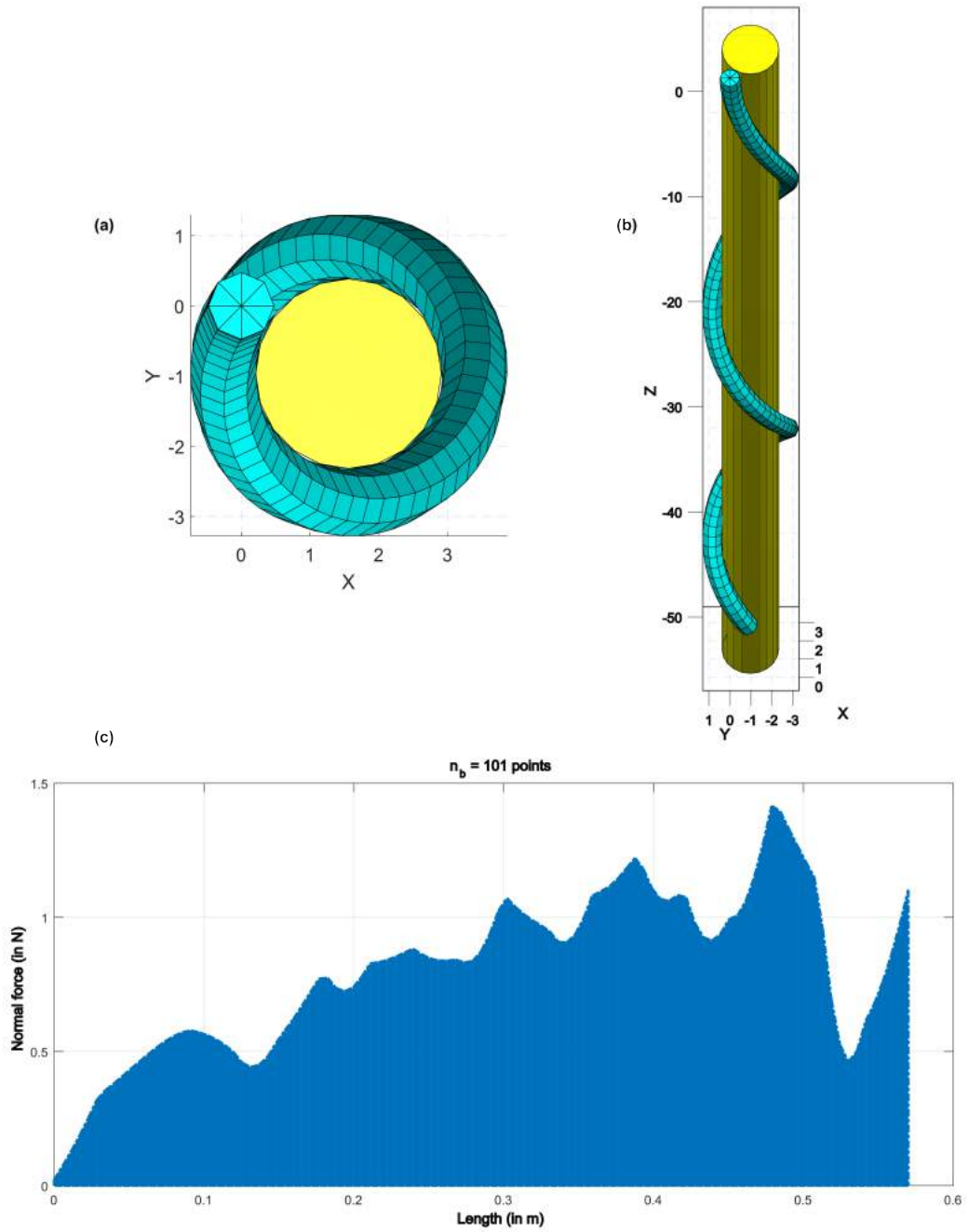

Figure 5.9: (a)Top view with cylindrical object (in yellow) when actuated to 16 psi with n_b = 101 points (b) View with az = -90 deg and el = 60 deg. where a perfect wrap is obtained (All axes are in cm) and (c) The normal force along the length of the actuator has no negative force after throughout actuator's length

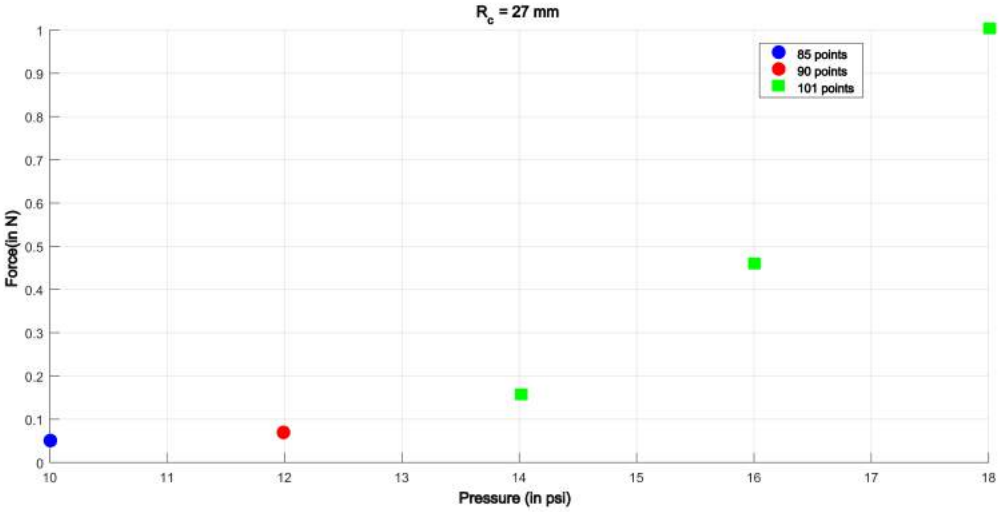

Figure 5.10: The normal force increases as the pressure is increased. The normal force for 10 psi and 12 psi is during case 2 (exhibit overhanging section)

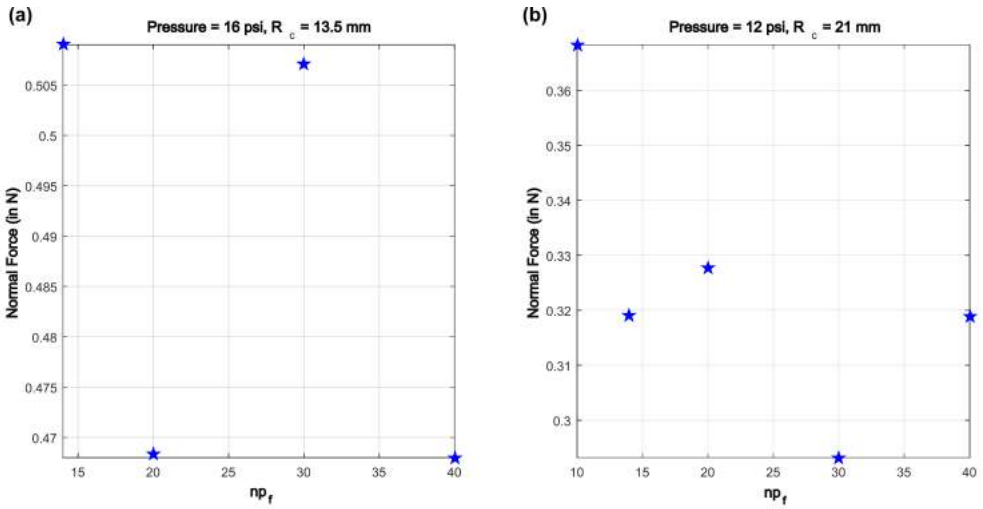

Figure 5.11: Variation of normal force with no of points force applied for sensitivity np_f

6 CONCLUSIONS AND FUTURE WORK

6.1 Conclusion

Soft continuum manipulators are increasingly popular as they have potential to safely interact with humans. This work takes initial steps towards application of FREE based spiral actuators for grasping long and slender objects and predicting whether the spiral actuator can grasp a given cylindrical object. This concept is deemed to be useful in handling delicate objects in industrial automation, space, underwater exploration and disaster management. The highlights of this work can be summarized below:

- Design of a FREE based spiral actuator with the available design space is presented. This can be used to convert an extending and rotating actuator to a spatial helical manipulator.
- Cosserat beam model is used on FREE to predict the final exact shape of the spiral actuator.
- An algorithm to estimate the normal forces exerted by the spiral actuator on the cylindrical object and different possible scenarios in execution of such a task are identified.

A soft spiral actuator has the capacity to carry large weights compared to its weight as it has the advantage of using its entire length for grasping, Fig.6.1(a),(b),(c) shows a spiral actuator with $\alpha = 60$ degrees and $\beta = 88$ degrees when actuated to 20 psi grasps a cylinder upto weight of 0.738 N.

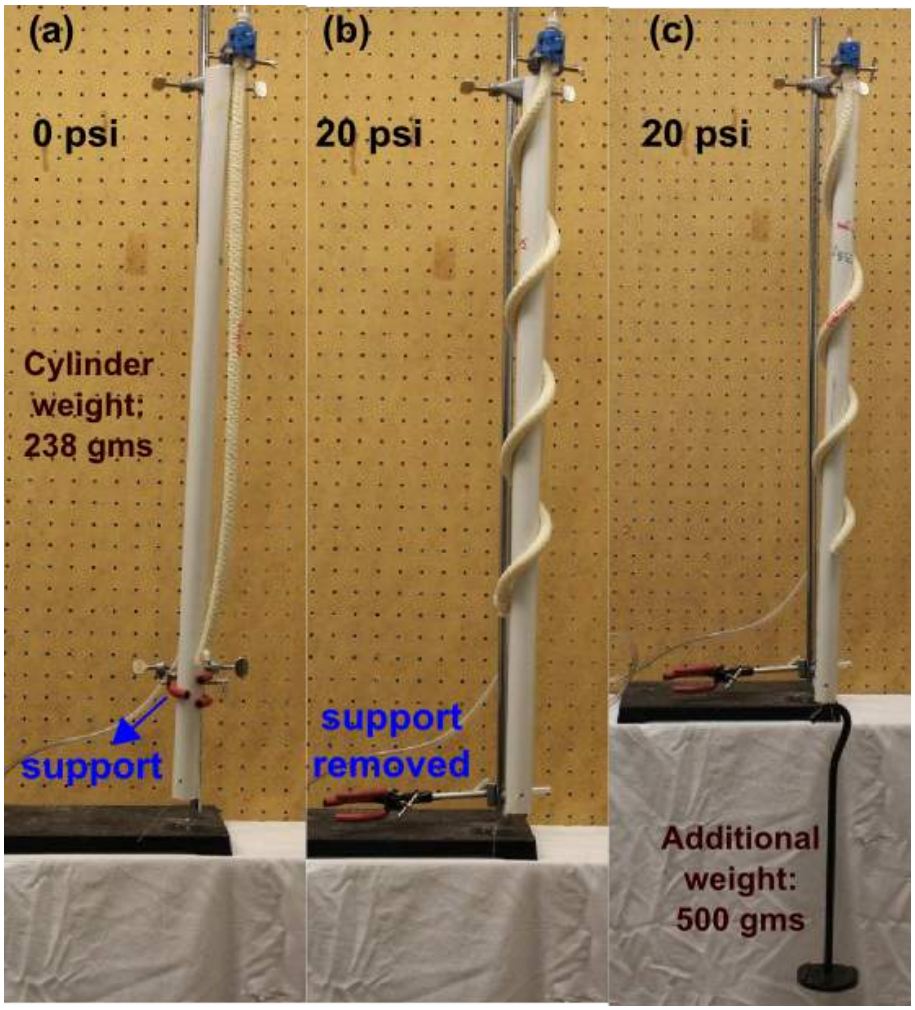

Figure 6.1: (a)Actuator at 0 psi with the cylindrical object placed tangentially with the help of a support (b) Actuator actuated to 20 psi leading to a stable grip, note the support is removed and (c) A stable grip with addition of extra load

6.2 Future work

The results presented in this work are preliminary investigations. Future work would be to explore the FREE design space to propose a range of diameters the spiral actuator can grasp based on the fiber angles. Second, to verify the proposed force estimation model, experiments need to be conducted to compare the analytical normal forces with the experimental results on different FREE compositions. Third, to add a friction model which can be used to predict the maximum weight of the object the actuator can grasp with the estimated normal force.

References

[1] S. Neppalli, B. Jones, W. McMahan, V. Chitrakaran, I. Walker, M. Pritts, M. Csencsits, C. Rahn, and M. Grissom, "Octarm-a soft robotic manipulator," in *Intelligent Robots and Systems, 2007. IROS 2007. IEEE/RSJ International Conference on*, pp. 2569–2569, IEEE, 2007.

[2] B. Mazzolai, L. Margheri, M. Cianchetti, P. Dario, and C. Laschi, "Soft-robotic arm inspired by the octopus: Ii. from artificial requirements to innovative technological solutions," *Bioinspiration & biomimetics*, vol. 7, no. 2, p. 025005, 2012.

[3] R. V. Martinez, J. L. Branch, C. R. Fish, L. Jin, R. F. Shepherd, R. Nunes, Z. Suo, and G. M. Whitesides, "Robotic tentacles with three-dimensional mobility based on flexible elastomers," *Advanced Materials*, vol. 25, no. 2, pp. 205–212, 2013.

[4] K. C. Galloway, K. P. Becker, B. Phillips, J. Kirby, S. Licht, D. Tchernov, R. J. Wood, and D. F. Gruber, "Soft robotic grippers for biological sampling on deep reefs," *Soft Robotics*, vol. 3, no. 1, pp. 23–33, 2016.

[5] D. Trivedi, C. D. Rahn, W. M. Kier, and I. D. Walker, "Soft robotics: Biological inspiration, state of the art, and future research," *Applied Bionics and Biomechanics*, vol. 5, no. 3, pp. 99–117, 2008.

[6] R. J. Webster and B. A. Jones, "Design and kinematic modeling of constant curvature continuum robots: A review," *The International Journal of Robotics Research*, 2010.

[7] J. Burgner-Kahrs, D. C. Rucker, and H. Choset, "Continuum robots for medical applications: A survey," *IEEE Transactions on Robotics*, vol. 31, no. 6, pp. 1261–1280, 2015.

[8] W. McMahan, V. Chitrakaran, M. Csencsits, D. Dawson, I. D. Walker, B. A. Jones, M. Pritts, D. Dienno, M. Grissom, and C. D. Rahn, "Field trials and testing of the octarm continuum manipulator," in *Proceedings 2006 IEEE International Conference on Robotics and Automation, 2006. ICRA 2006.*, pp. 2336–2341, IEEE, 2006.

[9] S. Sanan, M. H. Ornstein, and C. G. Atkeson, "Physical human interaction for an inflatable manipulator," in *2011 Annual International Conference of the IEEE Engineering in Medicine and Biology Society*, pp. 7401–7404, IEEE, 2011.

[10] S. Sanan, J. B. Moidel, and C. G. Atkeson, "Robots with inflatable links," in *2009 IEEE/RSJ International Conference on Intelligent Robots and Systems*, pp. 4331–4336, IEEE, 2009.

[11] M. T. Tolley, R. F. Shepherd, B. Mosadegh, K. C. Galloway, M. Wehner, M. Karpelson, R. J. Wood, and G. M. Whitesides, "A resilient, untethered soft robot," *Soft Robotics*, vol. 1, no. 3, pp. 213–223, 2014.

[12] N. W. Bartlett, M. T. Tolley, J. T. Overvelde, J. C. Weaver, B. Mosadegh, K. Bertoldi, G. M. Whitesides, and R. J. Wood, "A 3d-printed, functionally graded soft robot powered by combustion," *Science*, vol. 349, no. 6244, pp. 161–165, 2015.

[13] R. Deimel and O. Brock, "A novel type of compliant and underactuated robotic hand for dexterous grasping," *The International Journal of Robotics Research*, p. 0278364915592961, 2015.

[14] K. Suzumori, S. Iikura, and H. Tanaka, "Development of flexible microactuator and its applications to robotic mechanisms," in *Robotics and Automation, 1991. Proceedings., 1991 IEEE International Conference on*, pp. 1622–1627, IEEE, 1991.

[15] J. R. Amend, E. Brown, N. Rodenberg, H. M. Jaeger, and H. Lipson, "A positive pressure universal gripper based on the jamming of granular material," *IEEE Transactions on Robotics*, vol. 28, no. 2, pp. 341–350, 2012.

[16] V. Wall, R. Deimel, and O. Brock, "Selective stiffening of soft actuators based on jamming," in *2015 IEEE International Conference on Robotics and Automation (ICRA)*, pp. 252–257, IEEE, 2015.

[17] J. K. Salisbury, "Whole arm manipulation," *Proc. of the 4th Int. Sympo. Robotics Research, 1988*, 1988.

[18] J. A. Mather, "How do octopuses use their arms?," *Journal of Comparative Psychology*, vol. 112, no. 3, p. 306, 1998.

[19] J. Bishop-Moser and S. Kota, "Towards snake-like soft robots: Design of fluidic fiber-reinforced elastomeric helical manipulators," in *2013 IEEE/RSJ International Conference on Intelligent Robots and Systems*, pp. 5021–5026, IEEE, 2013.

[20] G. Krishnan, J. Bishop-Moser, C. Kim, and S. Kota, "Kinematics of a generalized class of pneumatic artificial muscles," *ASME Journal of Mechanisms and Robotics*, vol. 51, p. 61801, 2015.

[21] S. S. Antman, "Nonlinear problems of elasticity, 1995."

[22] D. C. Rucker and R. J. Webster, "Deflection-based force sensing for continuum robots: A probabilistic approach," in *2011 IEEE/RSJ International Conference on Intelligent Robots and Systems*, pp. 3764–3769, IEEE, 2011.

[23] G. Krishnan, "Kinematics of a new class of smart actuators for soft robots based on generalized pneumatic artificial muscles," in *Intelligent Robots and Systems (IROS 2014), 2014 IEEE/RSJ International Conference on*, pp. 587–592, Sept 2014.

[24] C.-P. Chou and B. Hannaford, "Measurement and modeling of mckibben pneumatic artificial muscles," *Robotics and Automation, IEEE Transactions on*, vol. 12, no. 1, pp. 90–102, 1996.

[25] C. S. Kothera, M. Jangid, J. Sirohi, and N. M. Wereley, "Experimental characterization and static modeling of mckibben actuators," *Journal of Mechanical Design*, vol. 131, p. 091010, 2009.

[26] D. Trivedi, A. Lotfi, and C. D. Rahn, "Geometrically exact models for soft robotic manipulators," *Robotics, IEEE Transactions on*, vol. 24, no. 4, pp. 773–780, 2008.

[27] D. C. Rucker, B. A. Jones, and R. J. Webster III, "A geometrically exact model for externally loaded concentric-tube continuum robots," *IEEE Transactions on Robotics*, vol. 26, no. 5, pp. 769–780, 2010.

[28] B. A. Jones, R. L. Gray, and K. Turlapati, "Three dimensional statics for continuum robotics," in *Intelligent Robots and Systems, 2009. IROS 2009. IEEE/RSJ International Conference on*, pp. 2659–2664, IEEE, 2009.

[29] R. M. Murray, Z. Li, S. S. Sastry, and S. S. Sastry, *A mathematical introduction to robotic manipulation*. CRC press, 1994.

[30] D. Rus and M. T. Tolley, "Design, fabrication and control of soft robots," *Nature*, vol. 521, no. 7553, pp. 467–475, 2015.